Supplemental materials

This file includes supplemental Figure legends, supplemental tables 1 and 2, supplemental Figures 1 through 4 and supplemental movie (1-16) captions

Supplemental Figure 1

Lack of Golgi disassembly during different phases of mitosis. Time is indicated in min:sec. Two nuclei in G2 (0 min) that subsequently underwent mitosis and were captured in prophase/metaphase (3 min), late anaphase (4 min, note the thread of chromatin still connecting the daughter chromosome sets) and telophase (6 min, strict $PacC^{27}$ nuclear localization had not yet been restored). No significant differences in Golgi organization were detectable.

Supplemental Figure 2:

The subcellular distribution of AnSec23-GFP foci is not affected by BFA treatment. Shown are simultaneously acquired (using a DV-2 Dual View) images of GFP and mRFP channels of the same cell photographed before and after BFA treatment. Note that mRFP-PH^{OSBP} bodies relocalize to large aggregates, whereas ERES do not undergo major changes.

Supplemental Figure 3:

The effects of the antimicrotubule agent benomyl on the distribution of the *trans*-Golgi. (A) through (C) Control experiment demonstrating that microtubules are depolymerised under our benomyl treatment conditions and subsequently reassembled after washout. (A) A germling expressing TubA-GFP photographed before treatment. Bar, 5 μm. (B) A TubA-GFP cell (maximal intensity projection of a 5-image z-stack series) photographed 10 min after addition of benomyl. (C) Single planes of TubA-GFP deconvolved z-stacks showing how cytoplasmic microtubules are reassembled (left) and mitotic spindles (Sp) formed (right) at 10 min after benomyl washout. (D) Dual channel imaging of mRFP-PH^{OSBP} GEs (red) and GFP-$PacC^{27}$ nuclei in a tip cell treated with benomyl for 30 min. Note the bulging of the hyphal tip and the polarization of the GEs ahead of the leading nucleus.

Supplemental Figure 4:

The effect of latrunculin B and benomyl on the subcellular distribution of AnSec23-GFP foci and of benomyl on GrhA-GFP structures. (A) Untreated cell control showing polarization of AnSec23-GFP foci illustrated by predominance of yellow/red colour near the tip in the pseudo-coloured hyphae. (B) These foci lose their polarization after latrunculin B treatment (30 min) and concentrate in bulged tips (C) upon benomyl treatment (38 min). (D) GrhA-GFP structures concentrate in the bulged tip (arrowed in the example) upon benomyl treatment (32 min).

Supplementary movie 1: Dynamics of mRFP-PH^{OSBP}-labelled Golgi equivalents in a growing hyphal tip. The filmed tip grows at 0.57 μm/min. Frames were taken every 10 sec. Fluorescent images are shown in inverted contrast to improve visualization of rings and tubular structures frequently undergoing exchange of membrane. The movie is displayed with x 60 acceleration. Note the faint cloud of material that labels the hyphal tip and which facilitates visualization of growth. The bar indicates 10 μm. Time scale is in min:sec

Supplementary movie 2: Another example of a rapidly growing tip (1.3 μm/min) expressing mRFP-PH^{OSBP} and photographed every 10 sec throughout an ~ 5 min period. Images are shown in inverted contrast. The distance between the most anterior GE and the apex is approximately 5 μm. The GEs seen are very dynamic and clearly undergo frequent exchange of material. The movie is accelerated 60 times. Time scale is in min:sec.

Supplementary movie 3: This hyphal tip corresponds to the cell shown in supplementary movie 1. The movie has been contrasted to maximise detection of material that apparently detaches from the most anterior Golgi bodies and reaches the apical dome plasma membrane. Time scale is in min:sec.

Supplementary movie 4: The dynamics of HypB^{Sec7}-GFP Golgi equivalents. The frames of this movie are projections of deconvolved z-stack series of a hyphal tip cell expressing HypB^{Sec7}-GFP. Z-stacks were taken every 2.6 sec over a total of 42 sec. Each z-stack series contains three planes. Note the frequent exchange of material between GEs connected by tubular structures.

Supplementary movie 5: The Golgi is not disassembled during mitosis. 4D, dual wavelength time lapse movie showing that there is no detectable reorganization of the Golgi during mitosis. Each frame is a maximal intensity projection of a z-stack series (5 images per channel) taken at the indicated time points (in min:sec).

Supplementary movie 6: Dynamics of AnSec23-GFP-labelled ERES in a growing hyphal tip. Frames were taken every 600 msec over a total of 19 sec. Fluorescent images are shown in inverted contrast to improve visualization of foci. Time scale is in sec: msec.

Supplementary movie 7: Dynamics of GrhA-GFP structures in a growing hyphal tip. Frames were taken every 800 msec over a total of 19 sec. Fluorescent images are shown in inverted contrast to improve visualization of foci. Time scale is in sec: msec.

Supplementary movie 8: The effects of BFA (300 μg/ml) treatment and washout in a strain expressing mRFP-PH^{OSBP}. The frames are maximal intensity projections of z-stack series (three planes each) of hyphal cells expressing mRFP-PH^{OSBP}, taken at the indicated time points (in min:sec). Also indicated are the frames taken after BFA addition (starting at 2 min after addition of the drug, time-point 11:32) and frames taken after BFA washout (at the 36:17 time-point). Note that this hypha completely stops apical extension after BFA addition, which also results in slight bulging of the tip. Also note the conspicuous aggregation of GEs into ‘brefeldin bodies’. Growth is resumed and the Golgi organization restored after BFA washout, but reversing the

effects of BFA takes clearly longer than upon treatment with 100 μg/ml of BFA (data not shown and see also below). The position of the bulged tip is indicated with an arrowhead and helps visualising the difference between the morphology of the tip after BFA-induced growth arrest and after resuming growth following BFA washout.

Supplementary movie 9: The effects of 100 μg/ml of BFA treatment and washout on the organization of the Golgi and apical growth as seen with HypB^{Sec7}-GFP. The frames of this movie are maximal intensity projections of z-stack series (three planes each), taken at the indicated time-points (in min:sec). Also indicated are the frames taken after BFA addition (starting 2 min after addition of the drug; time-point 10:30) and the frames taken after BFA washout (at the 39:22 time-point). Note that at this BFA concentration growth is slowed down but not arrested after BFA addition (the position of the tip during the BFA treatment is indicated with a filled arrowhead). As in the case of mRFP-PH^{OSBP} strains, GEs coalesce into large aggregates and BFA washout results in resumption of normal growth and reorganization of the Golgi.

Supplementary movie 10: BFA (300 μg/ml) treatment and washout in a strain co-expressing mRFP-PH^{OSBP} and GFP-PacC^{27}, showing that the BFA bodies are not adjacent to the nuclei. The frames of this movie are maximal intensity projections of dual wavelength z-stack series (GFP and mRFP filter sets; four planes for each channel), taken at the indicated time-points (in min:sec). Also indicated are the frames taken after BFA addition (starting 2 min after addition of the drug; time-point 16:08) and those taken after BFA washout (starting at the 48:15 time-point). Note that the Golgi depolarizes and aggregates into BFA bodies that do not show any evident relationship with nuclei. Also note that two hyphae undergo mitosis in the presence of BFA, and that brefeldin bodies remain intact during mitosis.

Supplementary movie 11: BFA (300 μg/ml) treatment and washout in a strain co-expressing mRFP-PH^{OSBP} and GrhA-GFP, showing that these two reporters localize to BFA-

induced aggregates but that these aggregates only very occasionally overlap. This relocalization is reversible as the two reporters recover their normal distribution after BFA washout. Note the characteristic bulging of the tip induced by this concentration of BFA. The frames of this movie are maximal intensity projections (three planes for each time point) of simultaneous dual wavelength z-stack series acquired with a Dual Viewer emission splitter, taken at the indicated time-points (in min:sec). Also indicated are the frames taken after BFA addition (starting 2 min after addition of the drug; time-point 8:48) and those taken after BFA washout (starting at the 33:25 time-point).

Supplementary movie 12:

BFA (300 µg/ml) treatment and washout in a strain co-expressing mRFP-PH^{OSBP} and AnSec23-GFP showing that, in contrast to late Golgi cisternae, ERES do not collapse upon BFA treatment. The frames of this movie are maximal intensity projections (three planes for each time point) of simultaneous dual wavelength z-stack series acquired with a Dual Viewer emission splitter, taken at the indicated time-points (in min:sec). Also indicated are the frames taken after BFA addition (starting 2 min after addition of the drug; time-point 9:00) and those taken after BFA washout (starting at the 35:36 time-point).

Supplementary movie 13: The effects of benomyl treatment and washout on the organization of the *trans*-Golgi, visualized with mRFP-PH^{OSBP}. The frames of this movie are maximal intensity projections of z-stack series taken at the indicated time-points (in min:sec). After benomyl addition, the tip changes its trajectory and subsequently bulges as reported, and the GEs concentrate in the bulged tip. Growth speeds up shortly after benomyl washout, and the GEs polarize into the newly emerging tip as normal apical extension proceeds. The frames of this movie are maximal intensity projections of z-stack series taken at the indicated time-points (in min:sec). Also indicated are the frames taken before and after benomyl addition (the first frame 'benomyl' was taken 10 min after benomyl addition, corresponding to time-point 18:26) and the first frame after washout corresponds to the (56:33 time-point).

Supplementary movie 14: The effects of latrunculin B (Lat B, 40 μg/ml)) treatment and washout on the organization of the *trans*-Golgi, visualized with mRFP-PH^{OSBP}. The frames of this movie are maximal intensity projections of z-stack series (6 planes each) taken at the indicated time-points (in min:sec). The depolarization and reduction in size of GEs resulting from Lat B treatment are most noticeable at the 43 and 49 min time-points, approximately corresponding to 30 min after Lat B addition. The frames taken before, after LatB addition and after LatB washout are indicated with text. Lat B arrests apical extension and results in tip bulging (indicated with a filled arrowhead). Two new tips (one is out of the focus; the one in focus is indicated with an open arrow) emerge subapically after washout. Note that GEs polarize into this nascent tip as soon as it emerges.

Supplementary movie 15: The effects of latrunculin B (Lat B, 40 μg/ml)) treatment and washout on the polarization of ERES, visualized with AnSec23-GFP. The frames of this movie are maximal intensity projections of z-stack series taken at the indicated time-points (in min:sec). Note how AnSec23 foci depolarize after Lat B addition and clearly repolarize towards the newly established polarity axis after LatB washout (60:34 timepoint). Frames after washout were taken every 10 min to minimize photodamage.

Supplementary movie 16: Dual wavelength time lapse sequence illustrating the mobility of early endosomes labelled with GFP-RabA^{Rab5} compared to GEs labelled with mRFP-PH^{OSBP}. Time is in min:sec.

Supplementary table 1: oligonucleotides used in this work

	Primer Name	Nucleotide Sequence (5´-3´)
1	FW HindIII CG mRFP	CCCAAGCTTCGGCCTCCTCCGAGGAC
2	Rev EcoRI GC mRFPns	GGGAATTCGCGGCGCCGGTGGAGTGG
3	New FW SmaI PH OSBP	TCCCCCGGGTTCGGGCTCGGCTCGAG
4	Rev Sma PH OSBP	TCCCCCGGGTCACGAATTCTTCTTCACAGC
5	GSP Sec7 (1)	CAGCCGAGCACGAGGACGGCGATATGCCAG
6	GSP Sec7 (2)	GCGCCGGCCGACGCTATGCTTGCGAGATGG
7	GFP Sec7 (A)	CCATCTCGCAAGCATAGCGTCGGCCGGCGCGGAGCTGGTGCAGGCGCTGGAGCC
8	GFP Sec7 (B)	CTAAAGCGGATATAAGAGAAGAAAACCAGTCGTCTGAGAGGAGGCACTGATGCG
9	GSP Sec7 (3)	GACTGGTTTTCTTCTCTTATATCCGCTTTAG
10	GSP Sec7 (4)	GGCCAAGTCACACATATTGACCGGAACTTC
11	PI4,5P2upBAM	GGATCCATGAGTAAAGGAGAAGAAC
12	PI4,5P2dwNsi	ATGCATCCATCGACCGGTCCCC
13	GSP1-Grh1 fw	GAGTTACCTTTGCAGTATGGAGCG
14	GSP2-Grh1 rev	TCCGGATTCCTTTTGCTCCTGCAATTGC
15	GSP3-Grh1 fw	TAGAAGAGATTTGTTTACGACTTGCAGC
16	GSP4-Grh1 rev	CGATGATTATCCCGCCGAATCCCC
17	FP1-Grh1 gfp pyrG fw	GCAATTGCAGGAGCAAAAGGAATCCGGAGGAGCTGGTGCAGGCGCTGGAGCC
18	FP2-Grh1 gfp pyrG rev	GCTGCAAGTCGTAAACAAATCTCTTCTAGTCTGAGAGGAGGCACTGATGCG
19	GSP1-sec23 fw	GCACAGTCTTTCGACCAGGAGGCCG
20	GSP2-sec23 rev	ACTCGTTCCAGAAACCGCAAGCC
21	GSP3-sec23 fw	TAAGTGCTGAGGTGATGCCGATTACG
22	GSP4-sec23 rev	GAGCCTTGATGACAAGGGAAGAGGC
23	FP1-sec23 gfp pyrG fw	GGCTTGCGGTTTCTGGAACGAGTGGAGCTGGTGCAGGCGCTGGAGCC
24	FP2-sec23 gfp pyrG rev	CGTAATCGGCATCACCTCAGCACTTAGTCTGAGAGGAGGCACTGATGCG

Supplementary Table 2: List of *A. nidulans* strains used in this study

strain number	Complete genotype	Origin or reference
540	*pabaA1 yA2; argB2*	
916	*pabaA1 yA2; areA^{c}366; pacC^{c}700; glc200*	E. Espeso
1117	*yA2; argB2; pantoB100*	E. Espeso
1385	*yA2; argB2[argB*-alcAp::gfp::rabA^{Rab5}]; kinAΔ::pyr-4; pantoB100*	Abenza e*t al.,* 2009
1399	*pabaA1 pyrG89 yA2; abpA::mrfp::pyrG^{fum}*	Araujo *et al.,* 2008
1434	*argB2[argB*-alcA^{p}::gfp::rabA^{Rab5}]; pantoB100; chaA1 nudA1*	Abenza e*t al.,* 2009
1739	*pyrG89; nkuAΔ::bar pyroA4*	H. Arst
1741	*wA4; inoB2 nkuAΔ::bar pyroA4*	H. Arst
2013	*wA4; inoB2 nkuAΔ::bar pyroA4[pyroA*-gpdA^{mini}::mrfp::PH^{OSBP}]; niiA4*	this study
2023	*pyrG89; sC12; choA1; chaA1 tubA::gfp*	B. Oakley
2060	*pabaA1 yA2; inoB2 pyroA4 [pyroA*-gpdA^{mini}::mrfp::PH^{OSBP}]; pacC^{c}700; niiA4, (glc200?)*	this study
2104	*pyrG89 hypB^{sec7}::gfp::pyrG^{fum}; nkuAΔ::bar pyroA4*	this study
2106	*argB2[argB*-alcA^{p}::gfp::rabA^{Rab5}]; inoB2 nkuAΔ::bar pyroA4[pyroA*-gpdA^{mini}::mrfp::PH^{OSBP}]; chaA1 niiA4 nudA1*	this study
2107	*argB2[argB*-alcA^{p}::gfp::rabA^{Rab5}]; inoB2 nkuAΔ::bar pyroA4[pyroA*-gpdA^{mini}::mrfp::PH^{OSBP}]; chaA1 nudA1*	this study
2120	*wA4; argB2[argB*-alcA^{p}::gfp::rabA^{Rab5}]; nkuAΔ::bar pyroA4[pyroA*-gpdA^{mini}::mrfp::PH^{OSBP}]; kinAΔ:pyr-4;*	this study
2121	*yA2; argB2[argB*-alcA^{p}::gfp::rabA^{Rab5}]; inoB2 nkuAΔ::bar pyroA4[pyroA*-gpdA^{mini}::mrfp::PH^{OSBP}]; pantoB100;niiA4*	this study
2122	*yA2; argB2[argB*-alcA^{p}::gfp::rabA^{Rab5}]; inoB2 nkuAΔ::bar pyroA4[pyroA*-gpdA^{mini}::mrfp::PH^{OSBP}]; kinAΔ:pyr-4; pantoB100; niiA4*	this study
2195	*argB2[argB*-alcA^{p}::gfp::rabA^{Rab5}]; nkuAΔ::bar pyroA4[pyroA*-gpdA^{mini}::mrfp::PH^{OSBP}]; pantoB100; chaA1 niiA4*	this study
2196	*wa4; argB2[argB*-alcA^{p}::gfp::rabA^{Rab5}]; nkuAΔ::bar inoB2 pyroA4[pyroA*-gpdA^{mini}::mrfp::PH^{OSBP}]*	this study
2243	*wA4; argB2; pyroA4[pyroA*-gpdA^{mini}::mrfp::PH^{OSBP}]; (niiA4?)*	this study
2306	*sec7::gfp::pyrG^{fum} pyrG89*; wA4; *nkuAΔ::bar pyroA4[pyroA*-gpdA^{mini}::mrfp::PH^{OSBP}]*	this study
2471	*pabaA1 yA2; argB2[argB*-gpdA^{p}::gfp::(PH^{PLCd})$_2$]*	this study
2472	*pabaA1 yA2; argB2[argB*-gpdA^{p}::gfp::PH^{PLCd}]*	this study

2508	wA4; *argB2[argB*-gpdA^{p}::gfp::PH^{PLCd}]; pyroA4[pyroA*-gpdA^{mini}::mrfp::PH^{OSBP}]; niiA4*	this study
2509	wA4; *argB2[argB*-gpdA^{p}::gfp::(PH^{PLCd})$_{2}$]; pyroA4[pyroA*-gpdA^{mini}::mrfp::PH^{OSBP}]; niiA4*	this study
2566	*pyrG89; nkuAΔ::bar pyroA4 ; Ansec23::gfp::pyrG^{fum}*	this study
2637	*pyrG89; nkuAΔ::bar pyroA4; grhA::gfp::pyrG^{fum}*	this study
2639	*pyrG89?;wA4; inoB2 nkuAΔ::bar pyroA4[pyroA*-gpdA^{mini}::mrfp::PH^{OSBP}]; Ansec23::gfp::pyrG^{fum}*	this study
2640	*pyrG89?; nkuAΔ::bar pyroA4[pyroA*-gpdA^{mini}::mrfp::PH^{OSBP}]; Ansec23::gfp::pyrG^{fum}*	this study
2642	*pyrG89?;wA4; inoB2 niiA4 nkuAΔ::bar pyroA4[pyroA*-gpdA^{mini}::mrfp::PH^{OSBP}]; grhA::gfp::pyrG^{fum}*	this study
2643	*pyrG89?; nkuAΔ::bar pyroA4[pyroA*-gpdA^{mini}::mrfp::PH^{OSBP}]; grhA::gfp::pyrG^{fum}*	this study

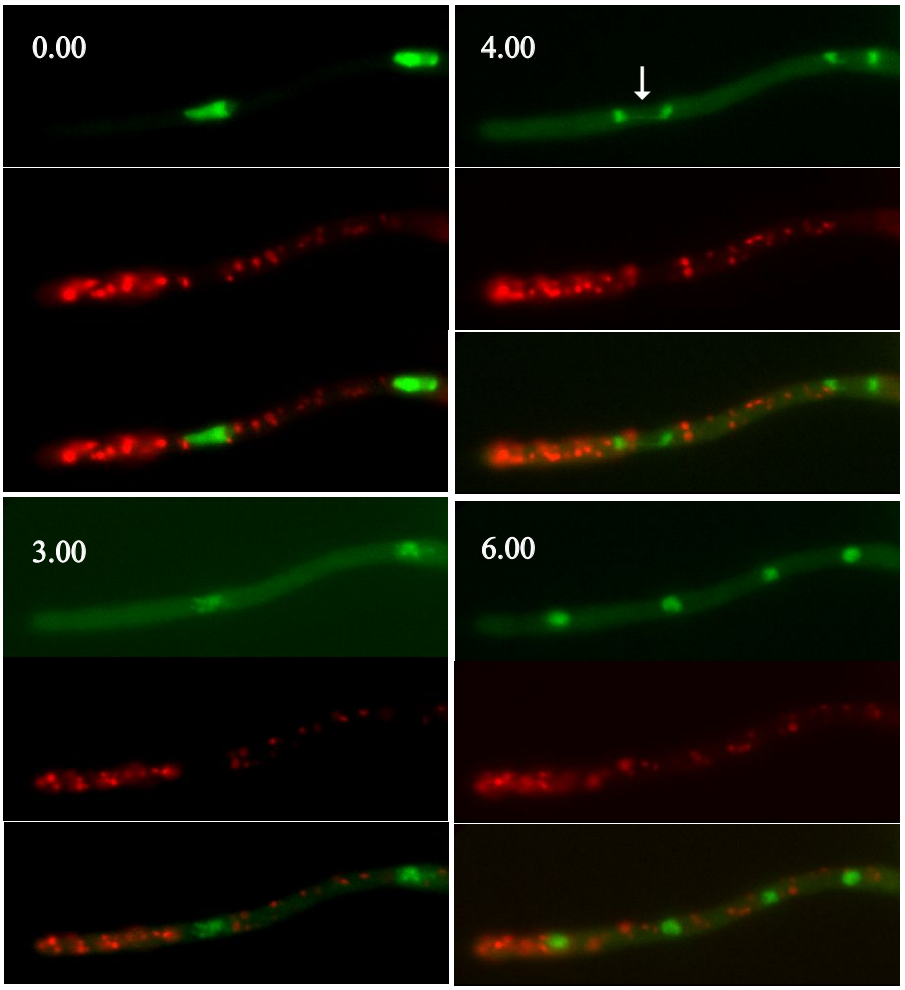

Pantazopoulou and Peñalva, Supplemental Fig. S1

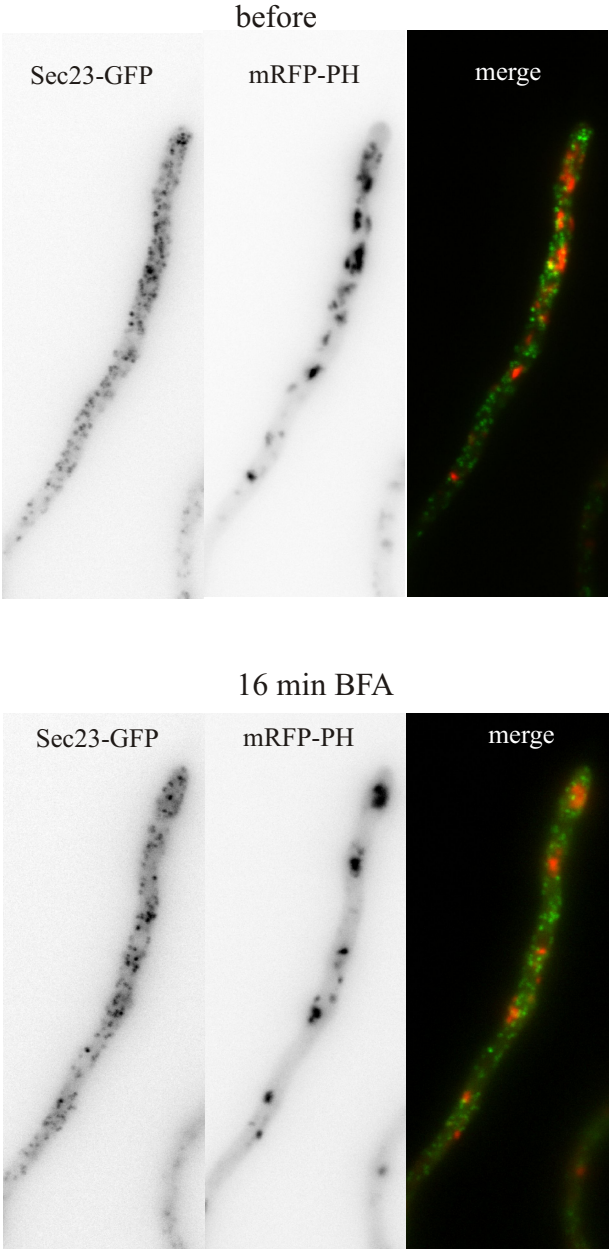

Pantazopoulou and Peñalva
Supplemental Fig. 2

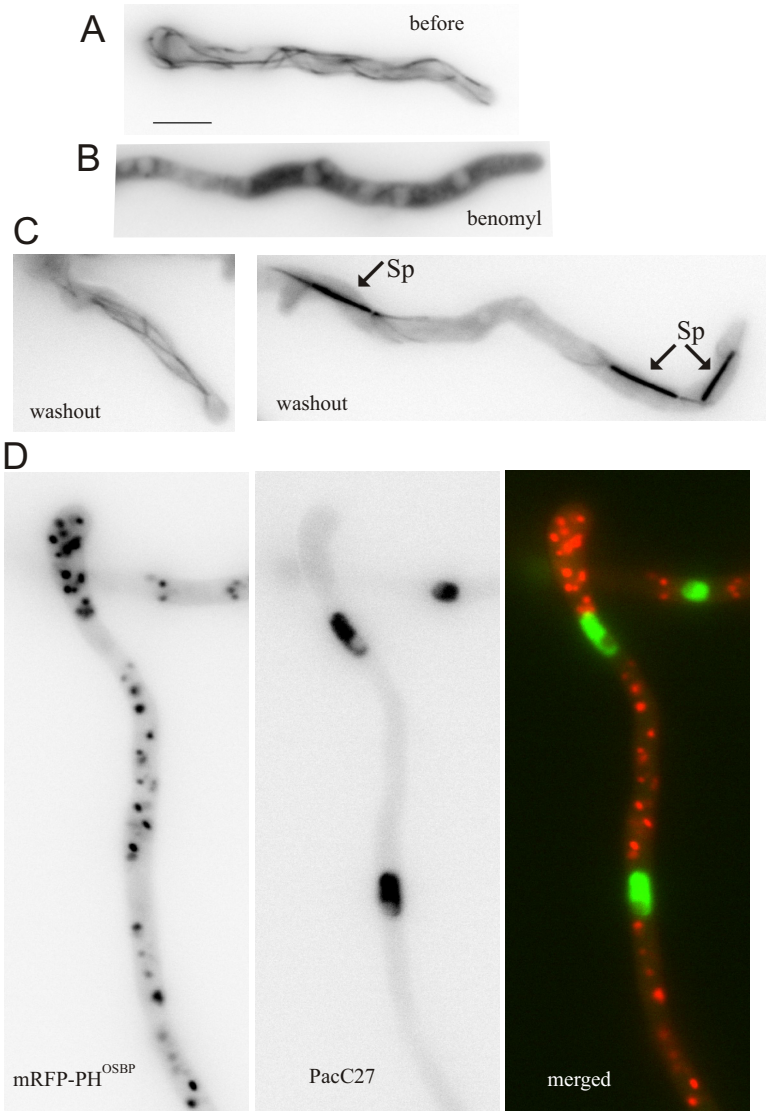

Pantazopoulou and Peñalva, supplemental Fig. 3

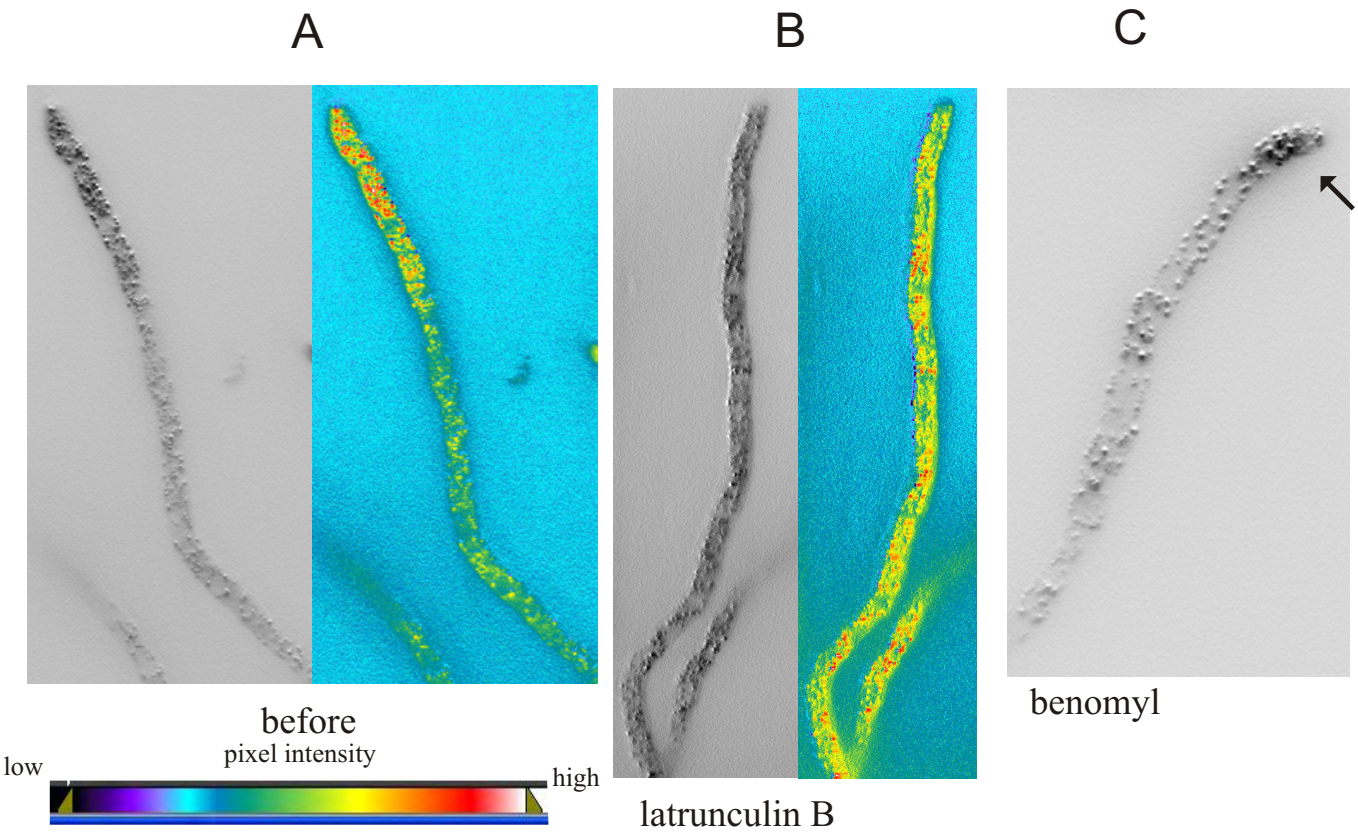

Panrazopoulou and Peñalva,
Supplemental Fig. 4